Available online at www.sciencedirect.com

SciVerse ScienceDirect

Magnetic Resonance Imaging 30 (2012) 978–992

MAGNETIC RESONANCE IMAGING

# The impact of sampling density upon cortical network analysis: regions or points

Jussi Tohka [a,*], Yong He [b], Alan C. Evans [c]

[a] Department of Signal Processing, Tampere University of Technology, P.O. Box 553, FIN-33101, Finland
[b] State Key Laboratory of Cognitive Neuroscience and Learning, Beijing Normal University, 100875 Beijing, China
[c] McConnell Brain Imaging Centre, Montreal Neurological Institute, McGill University, Montreal, Quebec, Canada H3A 2B4

Received 11 August 2011; revised 26 November 2011; accepted 14 February 2012

**Abstract**

The choice of representation has a fundamental influence on the network analysis results of an empirical data set. The answers to two basic questions — how to define a node and how to define an edge between a pair of nodes — are not obvious in the network analysis of brain imaging data. We considered the first question in the case of magnetic resonance imaging (MRI)-based cortical thickness networks. We selected network nodes to represent vertices of a cortical surface mesh or cortical brain regions. The first network represents the maximal level of detail available in the analysis of cortical thickness networks, while the latter network represents the typical level of detail in the current network analysis studies. We compared the network analysis results between these two representations. The basic network measures behaved approximately as expected when the level of detail increased. However, the overall connectivity of nodes was greater in the vertex level, degree of clustering was smaller in the vertex level, and the node centralities were different between the levels. Further, many parameters of vertex-level network were more robust to the selection of the correlation threshold used to define the edges of network. We conclude that albeit many qualitative network properties were consistent between the two resolution levels, the vertex-level resolution revealed details that were not visible at the regional-level networks, and this additional detail could be useful for some applications. Finally, a similar methodology as the one used here could be used to study effects of the sampling density in other brain-imaging-based networks, for example, in resting-state functional MRI.


*Keywords:* Complex networks; Cortical thickness; Magnetic resonance imaging; Small world; Graph theory; Image analysis

## 1. Introduction

The analysis of various complex networks derived from three-dimensional images of human brain has become a topic of emerging interest in neuroscience. The characterizations of the architecture of such complex networks can reveal general principles of structural and functional organization in the human brain and increase our understanding of how the human brain is capable of generating and integrating information from multiple sources in real time [1]. There exist several interesting properties of these networks — such as small-world properties, degree distributions and the centrality of the network nodes — that can be derived based on the graph theoretical analysis of these networks [2].

Most studies of complex brain networks in human have focused upon exploring connectivity patterns under functional brain states [3]. Anatomical connectivity networks have been derived based on magnetic resonance imaging (MRI)-based cortical thickness measurements [4–6], local gray matter volumes [7], regional cortical surface area [8] or diffusion MRI [9–12]. This work is related to Ref. [4], where an anatomical connectivity network was constructed through MRI-based cortical thickness measurements and the small-world property of the studied network was demonstrated. Cortical thickness was chosen as a morphometric feature because it reflects the size, density and arrangement of cells (neurons, neuroglia and nerve fibers) [13]. Moreover, as discussed in detail in Ref. [4], it has been suggested that interregional statistical associations in cortical thickness

* Corresponding author. Tel.: +358 40 1981497; fax: +358 3 31154989.
*E-mail address:* jussi.tohka@tut.fi (J. Tohka).

0730-725X/$ – see front matter © 2012 Elsevier Inc. All rights reserved.
doi:10.1016/j.mri.2012.02.029

provide important connectivity information in the human brain [14].

In Ref. [4], the cortex was segmented into 54 regions based on a brain atlas, and a 54×54 regional connectivity graph was constructed and studied. The cortical thickness for a given region was computed by averaging more local surface mesh-based measurements of the cortical thickness in each subject. Two regions were considered to be anatomically connected if there was a significant correlation of cortical thickness between the regions across a population of 124 normal brains. The coarse anatomical parcellation of the human cortex into 54 regions suggests that there are functional and anatomical variations within a region. Also, the anatomy of the human cerebral cortex is highly individual, and there is no single acceptable strategy for the cortical parcellation. Particularly, the validity of the atlas-based parcellation depends on the suitability of the applied atlas. This is an instance of the general problem of encoding brain imaging data into a network represented by nodes and edges between them. The problem of selecting a set of nodes for the network is already a very challenging problem in brain image analysis [15] and also in other applications [16]. Moreover, the node set selection will potentially affect the results and interpretations of the complex network analysis [16].

The 'node selection' problem has received some attention in brain imaging literature. In Ref. [17], the authors found significant differences in various topological parameters (e.g., small-worldness and degree distribution) between the functional MRI (fMRI)-based resting state connectivity networks derived based on different anatomical atlases. The influence of the atlas choice on the topological parameters of networks derived based on cortical thickness and regional cortical surface area was addressed in Ref. [8], where the authors found differences in various parameters due to the selected parcellation scheme. In Ref. [12], a more general choice of nodes question was addressed in the context of anatomical networks derived from diffusion tensor imaging and high-angular-resolution diffusion imaging by studying networks at different scales of representation varying from 82 to 4000 nodes. It was concluded that while binary conclusions about the network organization were unaffected by spatial scale, the quantitative values of various network parameters varied considerably with the scale of representation. Thus, it was recommended that the comparison of network parameters across studies must be made with a reference to the scale of representation.

In the case of MRI-based cortical thickness networks, the anatomical precision of the network is limited by the number of surface mesh points (vertices) at which the cortical thickness is estimated. The purpose of the present work is to compare the results of a coarse regional-level network (54 nodes; called $V$-node network in this paper) analysis and a fine surface-point or vertex-level network (40,962 nodes; called $N$-node network in this paper) analysis. Thus, in effect, we compare a standard network formed based on an anatomical atlas to a network that has maximally fine scale for this application. We report similarities and differences of various network parameters (connectivity patterns, degree distributions, small-world parameters and betweenness) between these two end points of the scale and show, in accordance to Ref. [12], that the binary conclusions were unaffected by the spatial scale of the network, but there were notable differences in individual parameter values. Moreover, many parameters of vertex-level $N$-node network were more robust to the selection of the correlation threshold used to define the edges of network.

## 2. Material and methods

### 2.1. Subjects, MRI acquisition and image processing

This study uses the International Consortium for Brain Mapping 152 data set which has been described elsewhere [18]. In brief, the subjects scanned were 152 unselected normal volunteers. Each subject gave written informed consent, and the Research Ethics Committee of the Montreal Neurological Institute (MNI) and Hospital approved the study. The scans of 28 subjects were excluded from the analysis due to left-handedness (14 subjects), unknown handedness (10 subjects) and failure of image processing (4 subjects). Of the remaining 124 right-handed subjects, 71 were male and 53 were female. Ages ranged from 18 to 39 years (mean age 24.38, standard deviation 4.25). MRI scans were performed on a Phillips Gyroscan 1.5-T superconducting magnet system with T1-weighted imaging sequence (three-dimensional fast field echo scan with 140–160 slices, 1-mm isotropic resolution, 18-ms time repetition, 10-ms time echo, flip angle of 30°).

The native MR images were first registered into stereotaxic space using a nine-parameter linear transformation [19]. The images were corrected for nonuniformity artifacts using the N3 algorithms [20]. The registered and corrected images were further tissue classified [21], and the fractional tissue content in each voxel was estimated [22,23]. The inner and outer gray matter surfaces were then automatically extracted from each MR volume using the Constrained Laplacian-based Automated Segmentation with Proximities algorithm [23,24]. Cortical thickness was measured in native-space millimeters using the linked distance between the white and pial surfaces at 40,962 vertices throughout the cortex [25]. The subjectwise thickness measurements were nonlinearly aligned to the standard template using two-dimensional (2D) surface registration [26].

### 2.2. Construction of cortical thickness networks

#### 2.2.1. N-node network

The statistical similarity in cortical thickness between two surface vertices was measured by computing the Pearson correlation coefficient across subjects, and $N \times N$ intervertex correlation matrix ($N$=40,962) of such connections was

acquired using the 124 brains included in this study. (Note that this correlation matrix is rank deficient.) Prior to the correlation analysis, a linear regression was performed at every vertex to remove the effects of age, gender, age–gender interaction and mean overall cortical thickness; the residuals of this regression were then substituted for the raw cortical thickness values. To form a simple undirected graph to be analyzed using methods from the complex network theory, the correlation matrix was thresholded at several levels $T^N \in \{0.3, 0.36, 0.39, 0.42, 0.45, 0.48\}$. A node pair with the absolute value of the correlation coefficient greater than $T^N$ was considered to be connected by an edge. The earlier work on regional-level networks [4] defined the connections based on the absolute values of correlation coefficients, and it is not an aim of the present work to analyze the role of negative correlations. Instead, we refer to Ref. [27] for further discussions about the role of negative correlations. The range of the studied correlation thresholds was selected based on the expected properties of the networks: we expect that the true anatomical connection network has a single connected component. Extending the upper limit of the studied correlation thresholds would lead to disconnected networks that clearly do not approximate the connection network. With the correlation threshold of $T^N=0.48$, 87% of the nodes belonged to the largest connected component. When $T^N>0.48$, this percentage started to decrease rapidly. On the lower limit, $T^N=0.30$, the characteristic path length was 2.85, which can be considered as a limiting value for the true anatomical correlation network given the bilateral nature of the human brain. The threshold $T^N=0.33$ was not studied as it was not an end point in the studied correlation range and it produced no false discovery rate (FDR)-adjusted $P$ value [28], i.e., this threshold was too low for any of the 40,961×40,962/2 hypothesis tests to show significant correlation after the FDR-based multiple comparisons correction.

#### 2.2.2. V-node network

A regional-level correlation matrix was constructed as in Ref. [4]. The labels of brain regions were transformed to the cortical surface by assigning the value of the voxel label to each vertex on the surface by registering each subject's MR images to a presegmented volumetric template using non-linear deformations [29]. The subjectwise cortical thickness values were averaged within a region, and 54×54 correlation matrix was constructed as described above for the vertex-level networks. This correlation matrix was then thresholded to create the regional or $V$-node network. We note that the operations of averaging the cortical thickness values and removing the effects of covariates are commutative. Hence, the regional-level correlation matrix is the same independent of the order of these operations. This is important because we want to study the $V$-node network, where the averaging takes place after the removal of the effects of covariates for the maximal comparability between the $V$-node and $N$-node networks, but in Ref. [4], the removal of the effects of covariates took place after the averaging.

### 2.3. Matching regional and vertex-level networks

Since the aim of this work was to study relationships between regional- and vertex-level networks, we needed a technique to match the correlation thresholds used to define the edges of the network. It is not obvious how such matching should be done because of possibly different probability distributions between regional and vertexwise correlation coefficients, and some possibilities and their limitations have been outlined in Ref. [33]. We applied two different matching techniques: *direct matching* and *FDR matching*. In the direct matching, the $V$-node networks were thresholded at the same thresholds as the $N$-node networks, i.e., $T^V=T^N$, where $T^V$ is the threshold for the $V$-node networks. We call the networks created this way *directly matched networks*. However, as we will demonstrate, it may not be reasonable to match the $N$-node and $V$-node networks at the same correlation threshold, but to correct for multiple comparisons. Therefore, we matched the $N$-node and $V$-node networks so that the $P$ value thresholds after the multiple comparisons corrections were equal. Here, the correction was based on FDR using the Benjamini–Hochberg procedure [28,34]. In this FDR matching, we set $p^V(T^V) = p^N(T^N)$, where $p^V$, $p^N$ denote the FDR-corrected $P$ value thresholds that are equivalent with the given correlation threshold. In other words, the threshold $T^V$ was selected so that the FDR-corrected $P$ value of $T^V$ (1431 comparisons when $V$=54) was equal to the FDR-corrected $P$ value of $T^N$ ($8.39\times10^8$ comparisons when $N$=40,962). The corresponding thresholds along with the FDR-corrected $P$ values are provided in Table 1. The $P$ values for the correlation coefficients were computed based on the $t$-transformation. These networks are called *FDR matched networks*.

The two matching procedures can be considered to provide upper and lower bounds of $T^V$ given $T^N$. Clearly, if the networks are directly matched, the possibility of a false-positive connection (i.e., an edge which is due to chance only) is much greater in the $N$-node networks. On the other hand, if the networks are FDR matched, the multiple comparisons correction may be more stringent with the $N$-node networks. This is because we can expect

Table 1
The correspondence between the correlation thresholds and FDR-adjusted $P$ values limit

| $T^N$ | FDR | $T^V$ |
|---|---|---|
| 0.30 | N/A | N/A |
| 0.36 | 0.5 | 0.23 |
| 0.39 | 0.1 | 0.29 |
| 0.42 | 0.05 | 0.31 |
| 0.45 | 0.005 | 0.38 |
| 0.48 | 0.0005 | 0.42 |

The $V$-node correlation thresholds are rounded to the first percentage that satisfies the FDR-corrected $P$ value.

the dependencies between the elements of $N\times N$ correlation matrix to be stronger than the dependencies between the elements of $V\times V$ correlation matrix. In these cases, the standard Benjamini–Hochberg procedure is known to be conservative [34,35] and thus, the proportion of false negatives can be conjectured to be greater with $N$-node networks.

We note that matching networks based on their edge density (also called sparsity, see Ref. [33]) would not be possible here. This is because $N$-node networks were intrinsically much more sparse than their regional counterparts. For example, the edge density of the $N$-node network with $T^N$=0.30 was 0.56 %, and the regional network with the same edge density would have only eight edges.

### 2.4. Graph theoretical measures

We studied several graph theoretical measures of the network topology including degree distributions, global efficiencies, clustering, small-worldness and centrality. There are several good reviews available explaining these measures, e.g., [2,15], and the purpose of this subsection is to give a brief overview and explain the choices made where necessary.

The degree of a node $i$, denoted here by $k_i$, is the number of edges connected to a node. When we refer specifically to $V$-node ($N$-node) networks, we use the superscript $V$ ($N$), writing, for example, $k_i^V$. The node degrees are not comparable between the $V$-node and $N$-node networks, and we compared the node degrees normalized by the number of nodes. The type of the network's degree distribution is an important concept in the network analysis for the classification of the networks into different categories [36]. In Ref. [4], it was found that the degree distributions of regional-level cortical thickness networks followed an exponentially truncated power law

$$P(k)\sim k^{-(\alpha-1)}exp(-k/k_0), \tag{1}$$

where $P(k)$ is the fraction of nodes having a degree greater than or equal to $k$ and $\alpha$ and $k_0$ are the parameters of the model (see Ref. [2]). Estimates of the model parameters were found by fitting the model (1) to the empirical cumulative distribution functions (cdfs) based on the least squares criterion. The parameter $\alpha$ is comparable between the $N$-node and the $V$-node networks, i.e., if we multiplied each $k_i^V$ by $N/V$ to account for the differences in the number of nodes, exactly the same estimate for $\alpha$ would be obtained as by using the original values $k_i^V$. The parameters $k_0$ are not comparable, and we compared them between $N$-node and $V$-node networks after multiplying $k_0^V$ by $N/V$, effectively resulting in normalization by the number of nodes.

To study the small-world properties of the networks, we adopted the procedure of Watts and Strogatz [37], where the clustering coefficients and characteristic path lengths of the network under study and a randomized version of it are compared, in a slightly modified form. Following Ref. [37], the clustering coefficient $c_i$ is here defined as the fraction of allowable edges that exist in the neighborhood of the vertex $i$ (see also Eq. [5] in Ref. [2] for an equivalent definition). If $k_i<2$, we set $c_i=0$ [2]. The average clustering coefficient is denoted by $<c>$. We denote by $d_{ij}$ the length of the shortest path between nodes $i$ and $j$. The characteristic path length $L$ is the average of $d_{ij}$ over all node pairs and for a disconnected network $L$ is infinite. To circumvent the problem, one can study the largest connected component of the network as, e.g., in Ref. [4]. However, to study the small-world properties of networks, a random network with the same degree of distribution as the original one needs to be constructed [37]. The generation of a random network corresponding to the largest connected component remains problematic because the randomized network may be disconnected even if the original network is connected. The average degree should fulfill $<k>^V>>\log(V)$ to guarantee (almost surely) that the random graph is connected [37]. A simple way to circumvent this problem is to study the global efficiency (here defined for $V$-node networks)

$$E_{glob}^V = 2\frac{\sum_{i,j}\left(1/d_{ij}^V\right)}{V(V-1)} \tag{2}$$

instead of the characteristic path length [38]. The global efficiency measures the efficiency of the information transmission in a parallel system, whereas the inverse of the characteristic path length measures the efficiency of the information transmission in a sequential system [39]. This makes global efficiency an attractive parameter to study in the analysis of the brain network topology because the brain is known to instantiate parallel processing [40]. Our small-world considerations will be based on global efficiency instead of characteristic path length.

As already mentioned, to establish the small-world character of a network, its global efficiency and average clustering coefficient were compared to the same parameters of a random network. Particularly, we studied quantities $\lambda=E_{glob}^{rand}/E_{glob}$ and $\gamma=\langle c\rangle/\langle c\rangle^{rand}$, where $E_{glob}^{rand}$ and $\langle c\rangle^{rand}$ are the global efficiency and the average clustering coefficient for a randomly rewired version of the original network. Here, we used the rewiring procedure of Ref. [41], which preserves the degree of each node of the network. For the small-world networks, $\lambda\sim 1$ and $\gamma>>1$ [37].

We evaluated the centrality of the node $i$ by betweenness centrality (BC) $b_i$. For node $i$, $b_i$ is defined as the number of shortest paths (geodesics) passing through $i$ [42]. We assumed that if there are $a$ shortest paths between a pair of nodes, then each node along these paths receives a score of $1/a$. The main advantage of the BC over the closeness centrality applied in Ref. [4] is that it is defined also for disconnected networks [43].

We used logarithms of BC values to visualize the centrality of nodes of $N$-node networks because BC values are often distributed according to a power law [44]. Because the BC distributions were different for different thresholds

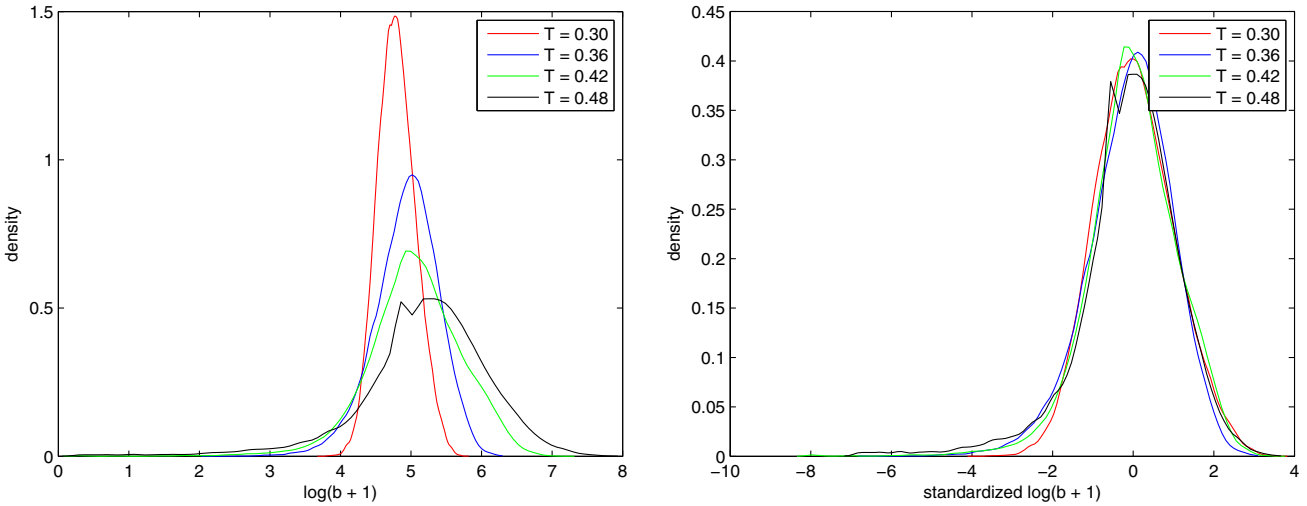


Fig. 1. Standardized logarithmic BC values of $N$-node networks. The Parzen estimates of the probability density functions (pdfs) of logarithms of the BC values ($lb_i$) are shown in the left panel. The Parzen estimates of the pdfs of the standardized logarithmic BC values ($lb_i$) are shown in the right panel. Pdfs of raw logarithmic BC values matched poorly between the thresholds, while standardization produced an excellent match. Note that normalizing BCs by dividing them by average (or median) BC would produce only a shift in the pdfs of the left panel, and this would be insufficient to ensure the match of the pdfs.

$T^N$ as is shown in Fig. 1, we standardized the logarithmic BC values to make the comparison between the thresholds easier. Let $lb_i^T = \log(b_i^T + 1)$ denote the logarithmic BC of the node $i$ at the correlation threshold $T^N$, where the addition of 1 before taking the logarithm ensures that $lb_i$ is nonnegative. Then, the standardized (logarithmic) BC was defined as

$$lb_i^T = \frac{lb_i^T - \text{median}_i\left(lb_i^T\right)}{1.483\text{median}_i\left(lb_i^T - \text{median}_j\left(ldb_j^T\right)\right)}. \quad (3)$$

This is a basic robust standardization procedure [45], meaning that it is not overly sensitive to outliers. Particularly, the denominator is known as robust *median absolute deviation* scale estimator [45]. This standardization produced an approximate match between the positive halves of the BC distributions (see Fig. 1). We chose a robust procedure due to outlying BC values that were abundant particularly at higher thresholds.

### 2.5. Standard errors of the correlation coefficients and average node degrees

To characterize and compare the variability within regional- and vertex-level thickness correlations due to the subject sample, we computed the jackknife estimates of the standard error (S.E.) of the correlation coefficients [30]. These were computed for each possible correlation coefficient separately, producing 40,961×40,962/2 S.E. estimates for the vertex-level analysis and 53×54/2 S.E. estimates for the regional-level analysis. The jackknife was selected as the estimator for the S.E. instead of more computationally intensive bootstrap techniques due to high computational demands for the vertex-level case; see Ref. [31] for an explanation of the relative computational ease of jackknife compared to bootstrap as well as the exact relationship of the two techniques. We computed also jackknife S.E. of average node degrees to clarify how the correlation variability affects networks properties. The extension of analysis of the correlation coefficient to the analysis of node degrees was relatively straightforward in the computational sense. However, the computational burden in the vertex level (see Section 2.6) prevented performing the analysis of the other network properties as done for regional networks in Ref. [8]. Also, it is unclear whether the jackknife technique, known to fail for the estimation of S.E. of sample quantiles (see Ref. [32]), is a suitable tool for assessing network measures. Therefore, we validated the jackknife technique by comparing it to bootstrap with a high number of bootstrap replications (3000) with the regional-level networks. The jackknife was found to be sufficiently reliable for the average degree (although, not surprisingly, some upward bias could be noticed) but failed for the maximum degree, and therefore, we limit our discussion to the S.E. of average degrees.

### 2.6. Implementation details

The network measures were computed based on customized Matlab code built on the Matlab Bioinformatics Toolbox (Mathworks, Natick, MA, USA) except that the BC was computed with the MATLAB BGL library version 4.0 [46]. The computation for a single vertex-level network (original or randomly rewired) required approximately from 12 h to 4 days of CPU time on a 3.0-GHz Intel XEON processor. The speed of the graph algorithms depends heavily on the number of edges in the networks, which explains the considerable timing differences between different networks. For rewiring, we used the Matlab

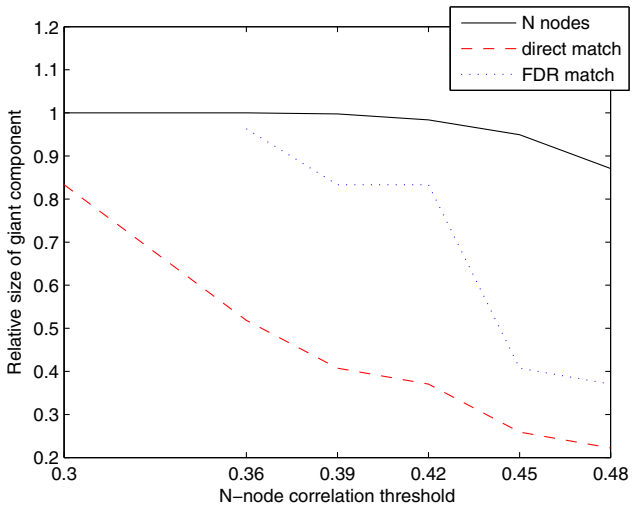


Fig. 2. The size of the largest connected component relative to the number of nodes in the network in percents. The regional-level network was much more prone to disconnection than the vertex-level network.

implementation available at http://www.cmth.bnl.gov/maslov/matlab.htm, which is slow for large networks and required several days of CPU time per network. The whole jackknife analysis required 10 days of CPU time.

## 3. Results

### 3.1. Standard errors of the correlation coefficients

In the vertex level, the average (over all possible vertex pairs) of the jackknife estimates for S.E. was 0.0918. In the regional level, the average was 0.0906. As expected, the S.E. was smaller in the regional level. Both of the values were close to the theoretical estimate of $1/\sqrt{123}\approx 0.0902$ for the S.E. of the correlation coefficient based on the normal theory. The S.E. values were stable across the cortical surface.

### 3.2. Connectivity and strongest connections

The sizes of the largest connected components of $N$-node and $V$-node networks are compared in Fig. 2. The $N$-node network was connected at $T^N=0.3$, and it was disconnected for higher thresholds. However, also for the higher thresholds, the largest connected component was large, and the second largest connected component was small (at $T^N=0.48$, 93 nodes corresponding to 0.2% of the total 40,962 nodes). As can be seen in Fig. 2, the $V$-node network was much more prone to disconnection even when FDR matched the $N$-node network. Particularly, for the thresholds greater than $T^V=0.31$, the giant component was too small to consider regional-level network as an approximation to an anatomical connectivity network. Thus, at the vertex level, the range of the correlation thresholds producing reasonable networks was greater. This observation indicates that there are network-analytical aspects of the brain which are not properly characterized by a regional-level network analysis.

To further characterize the additional detail visible at the vertex level, we computed the number of edges in the $N$-node network within each region $V_i$ of the applied atlas and compared it to the maximum number of possible edges in this region $W_i(W_i-1)/2$, where $W_i$ is the cardinality of $V_i$. The average ratio of the number of actual intraregional edges to the number of possible intraregional edges in the $N$-node networks varied between 4.4% (for $T^N=0.30$) and 1.4% (for $T^N=0.48$), with the maximum ratio of 16.1% in left precuneus for $T^N=0.30$. The negative correlation of the region size (in terms of $W_i$) and the fraction of realized intraregional edges was notable: it varied between −0.40 (for $T^N=0.48$) and −0.43 (for $T^N=0.36$).

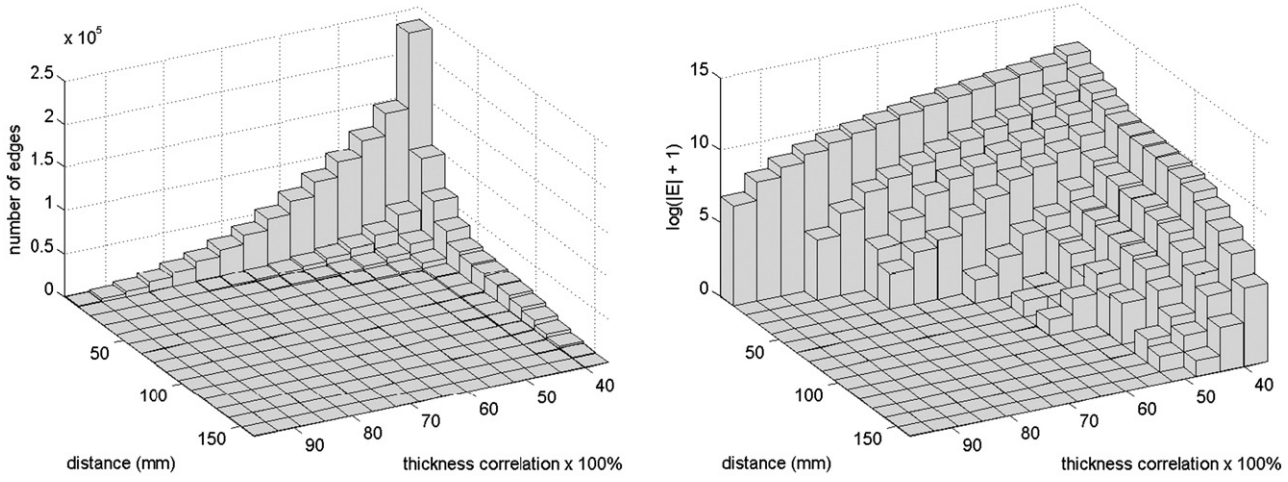


Fig. 3. Thickness correlation and geometrical distance between nodes in the $N$-node correlation matrices. The left (right) panel shows 2D histogram of the number of edges $|E|$ (log(|E|+1)) associated with a specified thickness correlation and geometrical distance between the two end nodes. On average, the connection strength decreased with increasing geometrical distance between node pairs.

Table 2
Statistics about positive and negative correlations as well as IHCs and SIHCs

| | Pos corr | Neg corr | Pos/neg ratio | IHC | SIHC | IHC/SIHC ratio |
|---|---|---|---|---|---|---|
| $T^N$=0.36 | 641,054 | 110,449 | 5.8 | 87,170 | 10,547 | 8.3 |
| $T^N$=0.42 | 394,321 | 27,561 | 14.3 | 13,725 | 3393 | 3.9 |
| $T^N$=0.48 | 265,674 | 10,215 | 26.0 | 2694 | 997 | 2.7 |
| Regional ($T^V$=0.31) | 76 | 28 | 2.7 | 58 | 18 | 3.2 |
| Regional ($T^V$=0.36) | 49 | 9 | 5.4 | 33 | 14 | 2.4 |
| Regional ($T^V$=0.42) | 32 | 3 | 10.7 | 17 | 11 | 1.5 |

The column 'Pos corr' ('Neg corr') gives the number of positive (negative) thickness correlations exceeding the threshold. Only those vertex-level interhemispheric and symmetric interhemispheric connections are counted that have a node-to-node distance larger than 1 cm to discount the influence of connections between nearby nodes near the midline. Symmetric interhemispheric connection has a reflection distance of at most 1 cm between its end vertices. The reflection distance between points ($x_1$, $y_1$, $z_1$) and ($x_2$, $y_2$, $z_2$) lying in opposite hemispheres in the stereotactic space was defined as $\sqrt{(x_1 + x_2)^2 + (y_1 - y_2)^2 + (z_1 - z_2)^2}$, where $x_1$, $x_2$ are the coordinates in the left–right axis. In other words, this distance is the distance between points in left hemisphere and in right hemisphere reflected with respect to the midsagittal plane.

The strongest edges — in terms of the absolute values of the correlation coefficient — between the nodes of the $N$-node networks were typically short-range connections as can be seen in Fig. 3. The correlation coefficient of the distance between the anatomical location of two nodes $D_{ij}$ and the absolute value of cortical thickness correlation between these nodes $corr(D_{ij},|r_{ij}|)$ was −0.38 (only the node pairs with $|r_{ij}|>0.36$ were accounted for). This indicates that the average 'connection strength' decreased with increased distance between the nodes. There was no qualitative difference between these observations and corresponding results in the earlier regional-level study [4]. Also, as in the regional-level analysis, a few long-range ($D_{ij}>75$ mm) connections were found: 42,284 with the correlation threshold $T^N$=0.36, 1195 with $T^N$=0.42, and 48 with $T^N$=0.48. The 48 long-range connections with $|r_{ij}|>0.48$ were most abundant between left middle frontal gyrus and left medial occipitotemporal gyrus (12 connections) and left cingulate and right superior temporal gyrus (4 connections). As in the regional-level networks, the long-range connections were typically between frontal cortex and temporal and occipital association cortices. However, also strong long-range connections from cingulate and insula to temporal and occipital association cortices were found.

Selected statistics about edges of the vertex-level networks are provided in Table 2, where also the same statistics about edges in the regional-level network are shown for reference. The edges with positive correlations were more abundant than the ones with negative correlations, with the positive/negative ratio increasing with the threshold. Note that, under FDR matching, the positive/negative ratio was greater in the vertex level, whereas, under direct matching, it was almost the same between the regional and vertex levels. Almost a full range of the anatomical distances was observed for the node pairs connected by an edge independent of the used correlation threshold. The maximal correlation coefficient (0.97) was with 0.65-mm distance [from the MNI coordinates of (3.98 mm 31.78 mm −5.42 mm) to (4.07 mm 32.33 mm −5.09 mm); a connection between neighboring nodes]. The minimal correlation coefficient (−0.74) was with 7.25-mm distance [from the MNI coordinates of (2.76 mm 31.47 mm −4.42 mm) to (−3.20 mm 27.60 mm −5.82 mm); interestingly, an interhemispheric connection). For the regional network, the maximum correlation was 0.67 (between left and right postcentral gyrus) and the minimum correlation was −0.47 (between right occipital pole and precuneus). This shows that the range of thickness correlations was extended in the vertex-level analysis as expected.

The numbers of interhemispheric and symmetric interhemispheric connections (IHCs and SIHCs) are also given in Table 2. The SIHCs were defined as the connections between homologous regions/vertices in the left and right hemispheres, which were speculated to be related to white matter

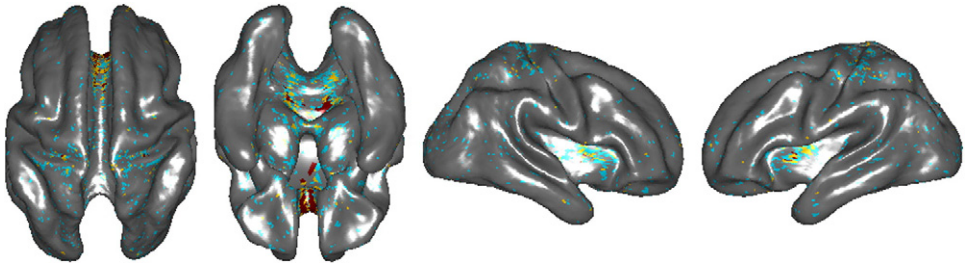

Fig. 4. Symmetric interhemispheric connections. Vertices having at least one SIHC at $T^N$=0.36, $T^N$=0.42 and $T^N$=0.48 are plotted in cyan, yellow and red, respectively. See Table 2 for the exact definition of SIHC. The SIHCs existed throughout the cortex; however, the strongest and most abundant were connections between insulas, cingulates and parahippocampal gyri.

tracts in the corpus callosum in Ref. [4]. For the exact definitions of IHCs and SIHCs, see Table 2. There existed both asymmetric and symmetric IHCs even at $T^N$=0.48. The relative number of SIHCs increased with the correlation threshold at both the regional and vertex levels. The vertices having at least one SIHC are shown in Fig. 4. The SIHCs existed throughout the cortex; however, strongest and the most abundant were connections between insulas, cingulates and parahippocampal gyri. We note that the threshold distance (1 cm) applied to define IHCs and SIHCs was rather arbitrary. Especially for SIHCs, a different threshold distance might have led to different results.

### 3.3. Degree distributions

The maximum and average degrees of the nodes of the networks are compared in Fig. 5. The normalized average and maximal node degrees were considerably greater in the matched $V$-node networks than in the $N$-node networks. The average and maximal degrees of the $N$-node networks varied between 13.5 ($T^N$=0.48) and 113 ($T^N$=0.30) and 266 ($T^N$=0.48) and 856 ($T^N$=0.30), respectively. The jackknifed standard errors for average degrees are listed in Table 3 (note that there is no normalization between regional and vertex levels in this table). For vertex-level networks, $\frac{s.e.<k>^N}{<k>^N}$ was smaller than 0.08 for all thresholds, which indicates a modest variability in the average degrees. Albeit nonnormalized average degrees in vertex-level networks were considerably greater than in the regional-level networks, the standard errors were comparable between the levels.

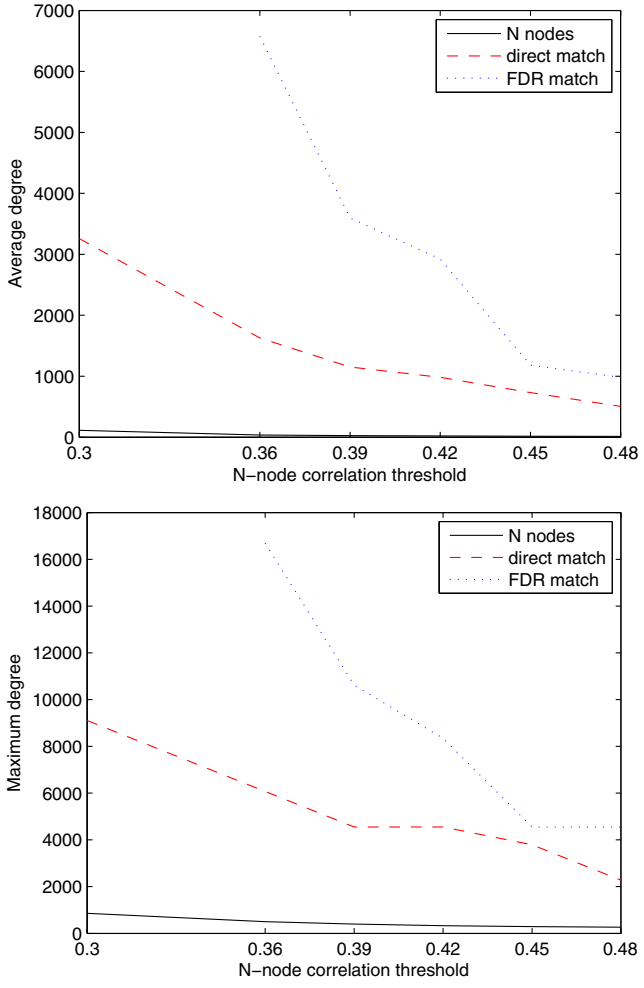


Fig. 5. The average (top) and maximal (bottom) node degrees of $N$-node networks compared to the average and maximal node degrees of the matched $V$-node networks. The node degrees of $V$-node networks have been multiplied by $N/V$ to account for different scale of the networks. This presentation scheme was selected in order to highlight the actual node degree values for $N$-node networks.

Table 3
Standard errors of average node degrees based on jackknife

| | | | | |
|---|---|---|---|---|
| $T^N$ | 0.30 | 0.36 | 0.42 | 0.48 |
| S.E. of $<k>^N$ | 5.05 | 2.50 | 1.47 | 0.92 |
| S.E. of $<k>^V$ | N/A | 1.41 | 1.09 | 0.47 |
| $T^V$ | N/A | 0.23 | 0.31 | 0.42 |

The networks were FDR matched.

The estimates of the empirical cdfs of node degrees along with exponentially truncated power law distributions fitted to the empirical cdfs based on the least squares criterion are displayed in Fig. 6. It can be seen (a) that the degree distributions of vertex-level networks did not follow the power law and (b) that exponentially truncated power law was a good approximation of the empirical distributions. Hence, these considerations are the same for the vertex- and regional-level networks (see Ref. [4]).

The values of parameters $\alpha$ and $k_0$ for different correlation thresholds are displayed in Fig. 7. The values of $\alpha$ were very stable for the $N$-node networks and more stable than for the $V$-node networks across the correlation thresholds. This suggests that the degree distribution analyses were robust to the choice of the correlation threshold in the vertex-level case. Also, the values for the parameter $\alpha^N$ matched well with the expectations based on the regional-level analyses (see Fig. 7) at the levels of the correlation threshold that seem most pertinent for the regional-level analysis (regional-level correlation thresholds close to 0.3 [4]). However, the parameter $\alpha^N$ had typically a higher value than what was expected based on $\alpha^V$. The cutoff values for the $N$-node networks were considerably lower than the cutoff values for the matched $V$-node networks multiplied by $N/V$ to account for difference in the number of nodes (see Fig. 7). This could be expected based on the results concerning average and maximal node degrees. The cutoff values for the $N$-node networks decreased with an almost linear trend with increasing correlation threshold.

### 3.4. Small-world properties

The characteristic path lengths ($L^N$) of the $N$-node networks were 2.85 ($T^N$=0.30), 4.37 ($T^N$=0.36), 5.84 ($T^N$=0.39), 8.39 ($T^N$=0.42), 13.26 ($T^N$=0.45) and 21.63

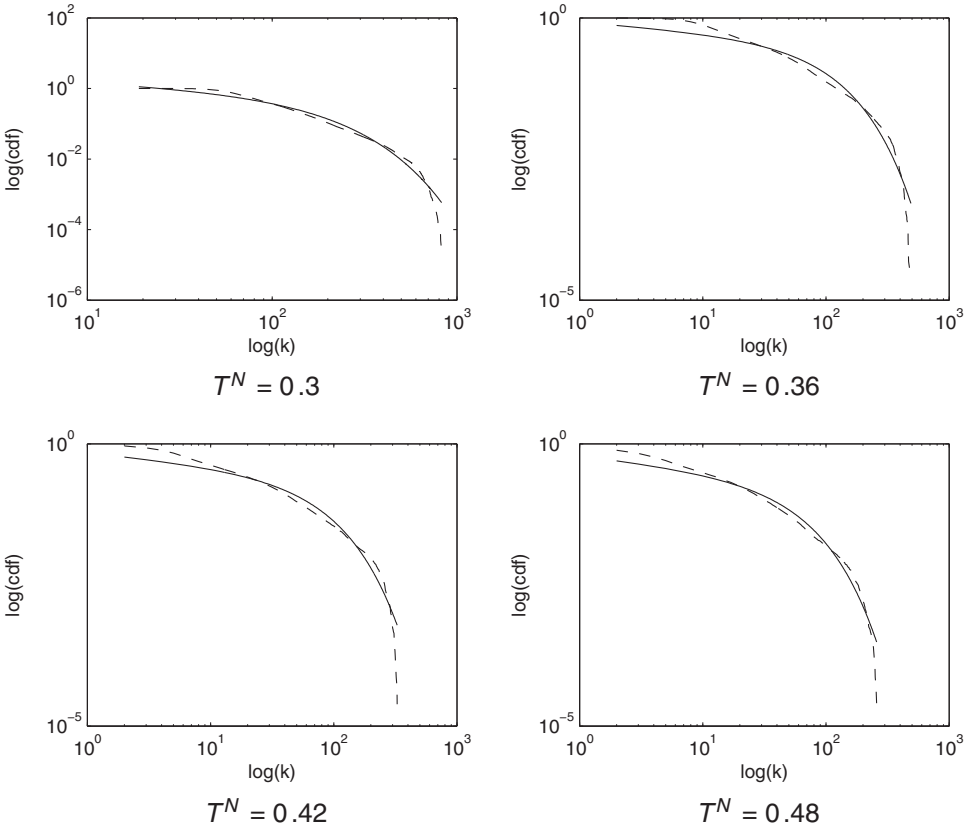


Fig. 6. Node degree distributions of the $N$-node networks. The empirical cdfs+ of node degrees are plotted with dashed lines, and the least squares fits of the exponentially truncated power law distribution are plotted with solid lines. The exponentially truncated power law distribution approximated well the empirical distributions. Only the $N$-node networks are considered as the corresponding figures for the regional-level networks have been presented in Ref. [4]. Figures for $T^N$=0.39 and $T^N$=0.45 are similar to figures for $T^N$=0.42 and $T^N$=0.48, and they are thus omitted.

($T^N$=0.48): these values were characteristic path lengths of the largest connected component. The global efficiencies are displayed in Fig. 8. The global efficiency $E^N_{glob}$ of the $N$-node network varied between 0.05 and 0.36, and it was in line with $E^V_{glob}$ of the directly matched $V$-node network. The mean (averaged over the six correlation thresholds) absolute difference between $E^N_{glob}$ and $1/L^N$ was 0.007, and the two quantities agreed almost perfectly with each other. However, as already noted, the characteristic path length is not defined for disconnected networks. Therefore, comparing characteristic path lengths across different resolutions would not be straightforward, at least in here where the size of the giant component varies considerably with the resolution (see Fig. 2).

The clustering coefficients are displayed in Fig. 8. The clustering coefficient of the $N$-node network increased until the correlation threshold reached $T^N$=0.39, and it remained at the same level for higher correlation thresholds. For example, under the FDR matching, the clustering coefficient of the $N$-node network had a value of 0.41 for $T^N$=0.42, and the clustering coefficient of the FDR-matched $V$-node network had a value of 0.25 for $T^V$=0.31. The clustering coefficients of $V$-node networks displayed a decreasing trend with increasing correlation threshold, which is explained by decrease in the connectivity of the networks (the $V$-node networks with $T^V$>0.31 had predominantly nodes with $k_i$ of 0 or 1 yielding $c_i$=0). This was in contrast to what was found for the $N$-node networks.

The quantities $\lambda^N$, $\lambda^V$, $\gamma^N$ and $\gamma^V$, where $\lambda^I=E^{I,rand}_{glob}/E^I_{glob}$, $\gamma^I=\langle c\rangle^I/\langle c\rangle^{I,rand}$ and $I$ denotes either $N$ or $V$, are shown in Fig. 8. The quantity $\lambda^N$ had a value close to one for thresholds $T^N$=0.30 and $T^N$=0.36, and then it started to increase, indicating that randomly rewired network had a higher global efficiency than the original network for higher correlation thresholds. However, the increase in $\lambda^N$ was more than counterbalanced by the increase in $\gamma^N$, meaning that the degree of clustering in the $N$-node networks was higher than in the randomly rewired $N$-node networks, and the $N$-node networks robustly displayed the small-world character in the sense that $\gamma^N>>\lambda^N$. This can be seen also in Table 4, where a summary measure $S^N=\frac{\gamma^N}{\lambda^N}$ (see Ref. [47]) is shown for different correlation thresholds along with the summary measures $S^V$ of the FDR-matched $V$-node networks. For most thresholds, $S^N$ and $S^V$ clearly exceeded the value of 1, which Ref. [47] suggested as the limit point for the small-world property. The $S^N$ values were higher than the matched $S^V$ values suggesting — at least in light of this simple summary measure — increased small-worldness of the

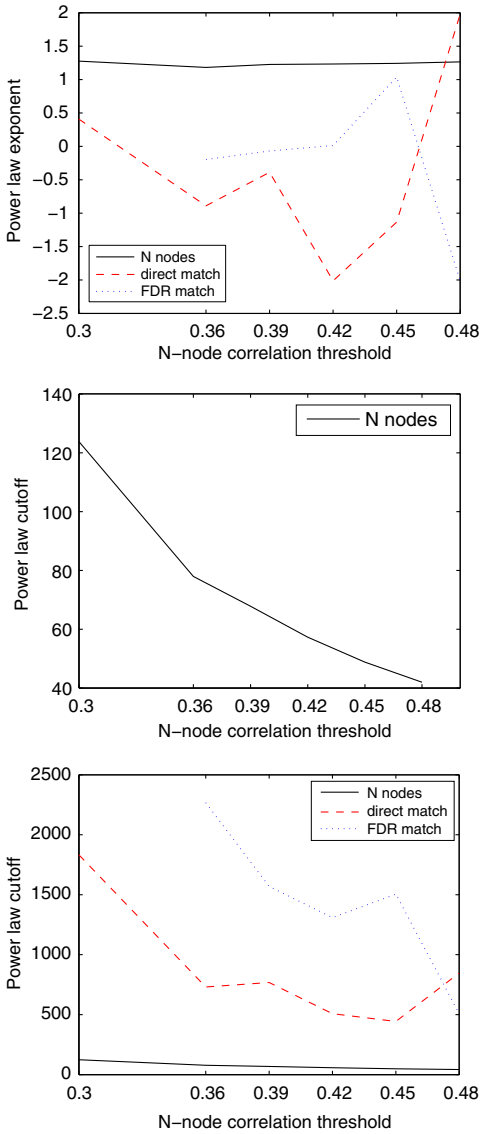


Fig. 7. Parameters $\alpha$ and $k_0$ of the exponentially truncated power law distributions. For $N$-node networks, the parameter $\alpha$ was extremely stable across the correlation thresholds, and $k_0$ decreased with an almost linear trend with correlation threshold. $k^V_0$ has been multiplied by $N/V$ to account for different scale of the networks.

vertex-level network. The summary measures $S^N$ were stable across the correlation thresholds, suggesting increased robustness of the detection of the small-world phenomenon.

### 3.5. Betweenness centrality

The standardized BC values [see Eq. (3)] projected on a population average surface are shown in Fig. 9. As is visible in Fig. 9, the most central nodes appeared in clusters at $T^N$=030 and at $T^N$=0.36, whereas they were more equally distributed throughout the cortex at $T^N$=0.48. The thresholds $T^N$=0.42 and $T^N$=0.48 showed more contrast in the centrality analysis than the lower thresholds. Especially the BC of zero was attributed to an increasing number of nodes: 6.80% of the nodes in the giant component received a centrality value of 0 at $T^N$=0.48, i.e., there were no shortest paths passing through them.

The hub nodes found in this analysis corresponded to some extent to 12 hub regions identified using a closeness centrality measure in Ref. [4]; see, e.g., Ref. [43] for discussions about different measures of node centrality. Precentral gyri, parahippocampal gyri and superior parietal lobule contained nodes with high vertex-level BC in agreement to the earlier regional-level analysis. Interestingly, high vertex-level BC was observed particularly in nodes in insula and cingulate. In the earlier regional-level analysis, the insula was connected to the rest of the network by a single link (from right insula to right cingulate), and the cingulate was not identified as a hub. Also, vertex-level BCs in middle and medial frontal gyri and in middle temporal gyrus were not particularly high here, but they were identified as hub nodes in the earlier regional-level analysis.

In Ref. [4], the hub nodes were identified based on the closeness centrality, while in the present work, we chose to use BC to cope with the networks that were not connected [42]. Therefore, in order to compare the vertex- and regional-level results, we reperformed the regional-level analysis using BC while averaging the BC values over the two hemispheres. This analysis identified 10 hub regions, the most important ones being precentral gyrus, middle temporal gyrus, superior parietal lobule, and inferior and superior frontal gyri, much in the same order as with the analysis based on the closeness centrality. The major differences were that the posterior central and middle frontal gyri were clearly hubs based on the regional closeness centrality, but not based on the regional BC. Qualitatively, the regional closeness centrality results seemed to match better with the vertex-level BC results.

## 4. Discussion

We have compared the cortical thickness networks where nodes represented brain regions (regional level) to the networks where the nodes represented individual points of the cortical surface mesh (vertex level). The basic conclusions were the same for both resolutions of representation: the networks displayed small-world character with the degree distributions following the exponentially truncated power law. However, many network properties appeared more stable across the correlation thresholds with the vertex-level resolution, and additional detail was visible in this finer level of representation. In particular, we found that the overall connectivity of nodes was greater in the vertex level, degree of clustering was smaller in the vertex level, small-worldness was increased in the vertex level and the node centralities were different between the levels.

One of basic findings was that vertex-level networks featured increased connectivity — referring to the increased relative size of the giant component of the network. In

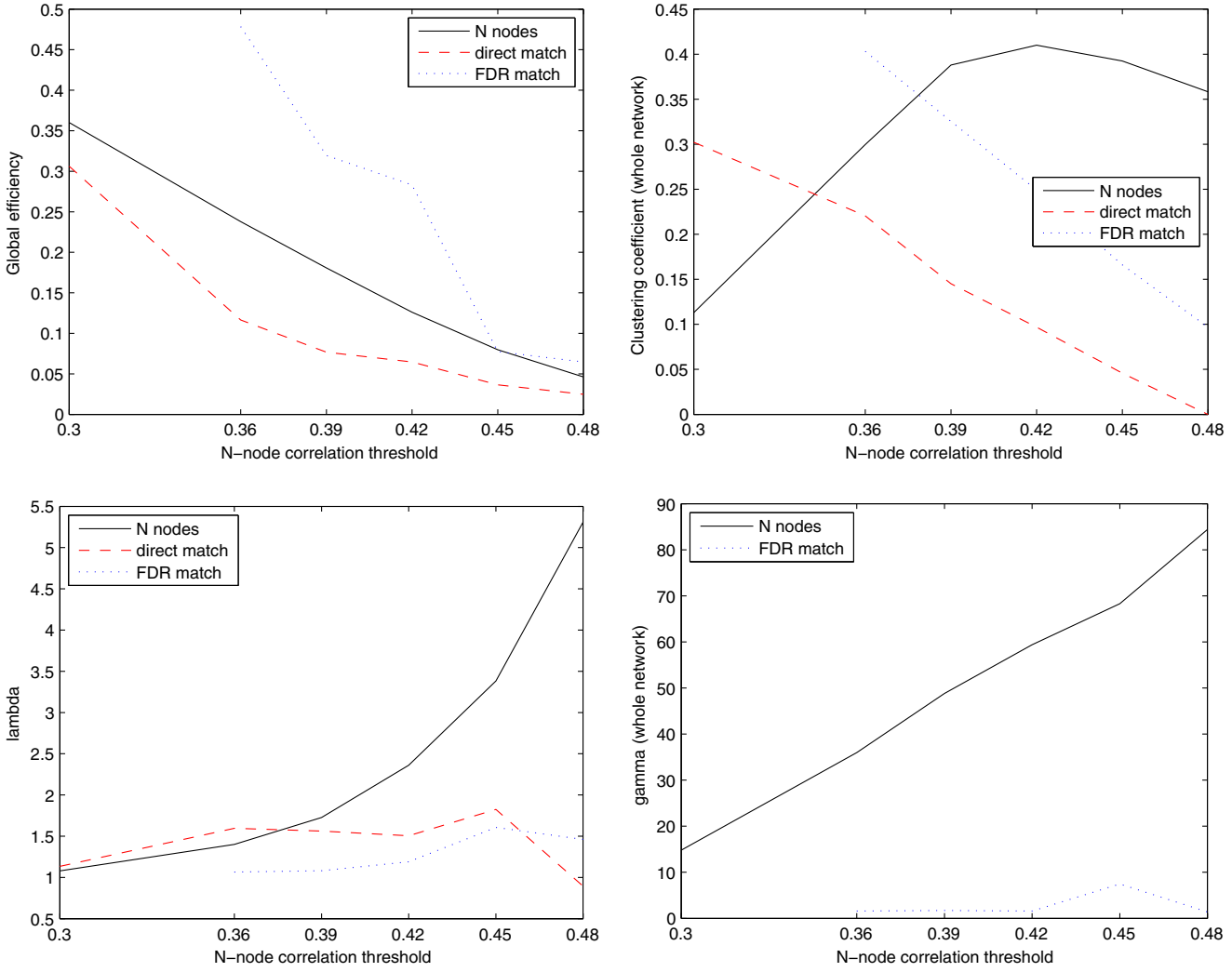


Fig. 8. The small-world properties. The global efficiency, clustering coefficient, $\lambda$ and $\gamma$ of the $V$-node and $N$-node networks as a function of the correlation threshold. $\gamma^V$ is plotted only under FDR matching because $<c>^{Vrand}$ was zero for high thresholds of $T^V$=0.45 and $T^V$=0.48. The $N$-node networks displayed small-world character in the sense that $\gamma^N > \lambda^N$.

addition, the number of realized edges within a region of the atlas was small compared to the potential number of edges within that region (see Section 3.2). These findings indicate that there existed a considerable variability of cortical thickness within a region of the applied atlas and, thus, there are likely to exist network-analytical aspects of the brain which are not completely characterized by a regional-level network analysis.

Table 4
Summary measures of small-worldness of the $N$-node networks ($S^N$) and $V$-node networks ($S^V$)

| | | | | | |
|---|---|---|---|---|---|
| $T^N$ | 0.36 | 0.39 | 0.42 | 0.45 | 0.48 |
| $S^N$ | 25.69 | 28.25 | 26.41 | 20.19 | 15.90 |
| $S^V$ | 1.48 | 1.59 | 1.33 | 4.65 | 0.94 |
| $T^V$ | 0.23 | 0.29 | 0.31 | 0.38 | 0.42 |

Correlation thresholds were FDR matched.

We observed a similar increase in the small-world summary measure with increasing number of nodes in networks to that observed in Ref. [12] for anatomical connectivity networks based on diffusion MRI. In Ref. [12], the authors attributed the observation to disproportionate increase in the clustering coefficient and discussed that causes for this phenomenon could include increased network sparsity, intrinsic properties of small-world networks and technical reasons. We did not observe a clear increase in raw clustering coefficient values between levels of representation. However, the clustering coefficient versus correlation threshold (that is directly related to network sparsity) mapping behaved differently between the levels of representation (see Fig. 8), and the parameter $\gamma$ — clustering coefficient normalized by a clustering coefficient of a random network — had a higher value in the vertex level. Thus, the increase in small-world summary measure might depend partially on the random network generation

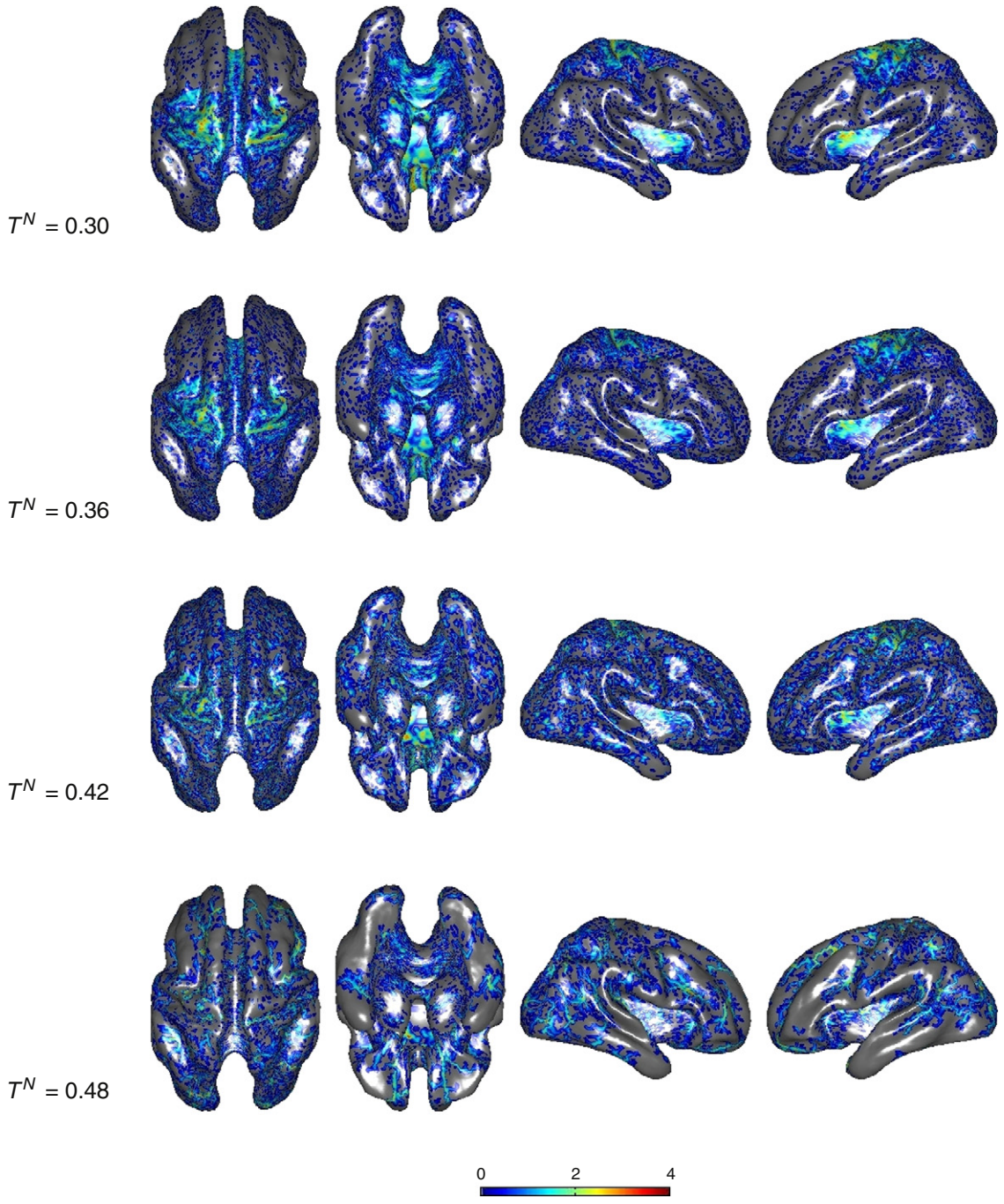


Fig. 9. Betweenness centrality. The standardized logarithmic BC values of the nodes for several correlation thresholds. Only nodes whose BC exceeds the median BC value are shown; other nodes are depicted in gray color. From left, superior, inferior, right and left views of the cortical surface are shown. The distribution of hub nodes appeared similar at $T^N$=0.30, $T^N$=0.36 and, $T^N$=0.42. At $T^N$=0.48, hubs were more evenly distributed throughout the cortex.

procedure or, on a more general level, the set of networks to which the observed network is compared for establishing the small-world property. Also, the small-world summary measures for the $N$-node networks were stable across different correlation thresholds. This suggests that an increased small-worldness in our case was not due to the increase in sparsity. We note that, besides the different aspects of anatomical connectivity studied, the criteria of small-worldness and random network generation differed between this work and Ref. [12], where small-world quantities were derived based on the characteristic path length instead of the global efficiency and Erdös–Renyi random graphs-based normalization was used instead of rewiring-based normalization.

There were substantial differences in the centrality of nodes between the regional and the vertex levels; some of the

brain regions which were central in the regional level (middle temporal and middle frontal gyri) did not contain hub nodes in the vertex level. On other hand, cingulate and insula contained central nodes in the vertex level but were not identified as hub nodes in the regional-level analyses. Although there were differences in the node centralities between the regional and vertex levels, the vertex-level hubs matched well to our expectations based on previous studies concerning anatomical and functional connections. High BC values in precentral gyrus agreed with a previous study in primates [48] that suggested that the motor cortex has widespread anatomical connections with parietal, prefrontal and cingulate cortical regions. Insula, parahippocampus and cingulate have been found to be highly interconnected with the prefrontal regions and subcortical regions [49]. In addition, the high BC in the primitive paralimbic and limbic cortical regions may provide evidence to support the 'preferential attachment,' an important concept in the network evolution in which new nodes are preferentially attached to the nodes that are already well connected [50]. Interestingly, hub regions identified here showed a large overlap with those found in functional networks of the human brain [51]. It could imply an association of morphological and functional organization in the brain. The differences between the centrality analysis results between the regional and vertex level indicate that there were variations in the cortical thickness within a brain region. While this does not nullify the regional network analysis results in any way, it is evidence that additional detail can be found at the vertex level.

A similar methodology as the one used here could be used to study effects of the sampling density in other correlation-derived brain-imaging-based networks, for example, in resting-state fMRI (rs-fMRI). Drawing direct conclusions about the sampling density effects on rs-fMRI networks based on the analysis of cortical thickness networks, or vice-versa, should however be avoided. This is because, albeit similar spatial patterns of functional and anatomical connectivity have been observed in specific networks [52], the mechanisms behind functional time-series correlations in rs-fMRI and cortical thickness correlations are different (although potentially related). A recent study [53] compared the results of the regional and voxel-based rs-fMRI network analysis. The overall conclusions of that study were similar to our conclusions concerning cortical thickness networks. In particular, Ref. [53] reported a trend for increased connectivity and greater small-worldness at increasing resolutions; however, increases were less extreme than in our analysis. In contrast, Ref. [54], also studying scaling effects on rs-fMRI networks, found a trend for higher resolutions to be associated with lower small-worldness when $\gamma$ and $\lambda$ were calculated using the same rewiring-based normalization as in this work. As speculated in Ref. [54], this inconsistency between the findings of the two studies may relate to different criteria used to match networks with different number of nodes and indicates that the selection of the matching criterion is an important methodological consideration in studies of sampling density effects on brain imaging networks.

Studies comparing different representations of connectivity networks derived based on brain imaging data are warranted because it is not obvious how to correctly define a network node at the current resolution of the brain imaging data — if there is a correct definition. This problem is much broader than just being brain imaging network related [16]. A closely related problem is the definition of a connection between a pair of nodes. We chose to ignore this problem almost entirely in this work and only repeated our analysis for varying correlation thresholds, which is the standard approach in the brain imaging network analysis. It might be that the weighted networks provide at least a partial answer to this problem. However, weighting edges based on the correlations they receive requires a choice of the correlation to weight mapping, which might be different for different applications. Moreover, there is no generally accepted method for a generation of a random network which replicates the desired properties of a given weighted network.

In summary, regional-level representation provided a smooth overall view to the cortical networks, while vertex-level representation provided more detail but probably included also details that were not interesting, e.g., connections between neighboring vertices. Interestingly, the jackknife estimates for S.E. of regional- and vertex-level correlation coefficients were similar, which suggest that, in this sense, the noise level was similar between the regional and vertex levels. The optimal resolution for the representation of cortical networks, if there is one, depends probably on the application, and probably, multiple levels of representation are useful as they provide complementary information.

## Acknowledgments

We thank Pierre Bellec, Felix Carbonell, John Chen and Budhachandra Khundrakpam for comments on earlier drafts. This work has been supported by the Academy of Finland (grant number 130275).

## References

[1] Sporns O, Chialvo DR, Kaiser M, Hilgetag CC. Organization, development and function of complex brain networks. Trends Cogn Sci 2004;8(9):418–25, http://dx.doi.org/10.1016/j.tics.2004.07.008.
[2] Newman M. The structure and function of complex networks. SIAM Rev 2003;45:167–256.
[3] Stam CJ, Reijneveld JC. Graph theoretical analysis of complex networks in the brain. Nonlinear Biomed Phys 2007;1(1):3, http://dx.doi.org/10.1186/1753-4631-1-3.
[4] He Y, Chen ZJ, Evans AC. Small-world anatomical networks in the human brain revealed by cortical thickness from MRI. Cereb Cortex 2007;17(10):2407–19, http://dx.doi.org/10.1093/cercor/bhl149.
[5] Chen ZJ, He Y, Rosa-Neto P, Germann J, Evans AC. Revealing modular architecture of human brain structural networks by using cortical thickness from MRI. Cereb Cortex 2008;18(10):2374–81, http://dx.doi.org/10.1093/cercor/bhn003.

[6] Chen ZJ, He Y, Rosa-Neto P, Germann J, Evans AC. Age-related alterations in the modular organization of structural cortical network by using cortical thickness from mri. NeuroImage 2011;56(1):235–45.
[7] Bassett DS, Bullmore E, Verchinski BA, Mattay VS, Weinberger DR, Meyer-Lindenberg A. Hierarchical organization of human cortical networks in health and schizophrenia. J Neurosci 2008;28(37):9239–48, http://dx.doi.org/10.1523/JNEUROSCI.1929-08.2008.
[8] Sanabria-Diaz G, Melie-García L, Iturria-Medina Y, Alemán-Gómez Y, Hernández-González G, Valdés-Urrutia L, Galán L, Valdés-Sosa P. Surface area and cortical thickness descriptors reveal different attributes of the structural human brain networks. Neuroimage 2010;50(4):1497–510, http://dx.doi.org/10.1016/j.neuroimage.2010.01.028.
[9] Hagmann P, Kurant M, Gigandet X, Thiran P, Wedeen VJ, Meuli R, Thiran J-P. Mapping human whole-brain structural networks with diffusion mri. PLoS One 2007;2(7):e597, http://dx.doi.org/10.1371/journal.pone.0000597.
[10] Iturria-Medina Y, Sotero RC, Canales-Rodríguez EJ, Alemán-Gómez Y, Melie-García L. Studying the human brain anatomical network via diffusion-weighted MRI and graph theory. Neuroimage 2008;40(3):1064–76, http://dx.doi.org/10.1016/j.neuroimage.2007.10.060.
[11] Gong G, He Y, Concha L, Lebel C, Gross DW, Evans AC, Beaulieu C. Mapping anatomical connectivity patterns of human cerebral cortex using in vivo diffusion tensor imaging tractography. Cereb Cortex 2009;19(3):524–36, http://dx.doi.org/10.1093/cercor/bhn102.
[12] Zalesky A, Fornito A, Harding IH, Cocchi L, Yücel M, Pantelis C, Bullmore ET. Whole-brain anatomical networks: does the choice of nodes matter? Neuroimage 2010;50(3):970–83, http://dx.doi.org/10.1016/j.neuroimage.2009.12.027.
[13] Narr KL, Bilder RM, Toga AW, Woods RP, Rex DE, Szeszko PR, Robinson D, Sevy S, Gunduz-Bruce H, Wang Y-P, DeLuca H, Thompson PM. Mapping cortical thickness and gray matter concentration in first episode schizophrenia. Cereb Cortex 2005;15(6):708–19, http://dx.doi.org/10.1093/cercor/bhh172.
[14] Lerch JP, Worsley K, Shaw WP, Greenstein DK, Lenroot RK, Giedd J, Evans AC. Mapping anatomical correlations across cerebral cortex (MACACC) using cortical thickness from MRI. Neuroimage 2006;31(3):993–1003, http://dx.doi.org/10.1016/j.neuroimage.2006.01.042.
[15] Rubinov M, Sporns O. Complex network measures of brain connectivity: uses and interpretations. Neuroimage 2010;52:1059–69, http://dx.doi.org/10.1016/j.neuroimage.2009.10.003.
[16] Butts CT. Revisiting the foundations of network analysis. Science 2009;325(5939):414–6, http://dx.doi.org/10.1126/science.1171022.
[17] Wang J, Wang L, Zang Y, Yang H, Tang H, Gong Q, Chen Z, Zhu C, He Y. Parcellation-dependent small-world brain functional networks: a resting-state fMRI study. Hum Brain Mapp 2009;30:1511–23, http://dx.doi.org/10.1002/hbm.20623.
[18] Watkins KE, Paus T, Lerch JP, Zijdenbos A, Collins DL, Neelin P, Taylor J, Worsley KJ, Evans AC. Structural asymmetries in the human brain: a voxel-based statistical analysis of 142 MRI scans. Cereb Cortex 2001;11(9):868–77.
[19] Collins DL, Neelin P, Peters TM, Evans AC. Automatic 3D inter-subject registration of MR volumetric data in standardized Talairach space. J Comput Assist Tomogr 1994;18(2):192–205.
[20] Sled JG, Zijdenbos AP, Evans AC. A non-parametric method for automatic correction of intensity non-uniformity in MRI data. IEEE Trans Med Imaging 1998;17(1):87–97.
[21] Zijdenbos A, Forghani R, Evans A. Automatic pipeline analysis of 3-D MRI data for clinical trials: application to multiple sclerosis. IEEE Trans Med Imaging 2002;21(10):1280–91.
[22] Tohka J, Zijdenbos A, Evans A. Fast and robust parameter estimation for statistical partial volume models in brain MRI. Neuroimage 2004;23(1):84–97.
[23] Kim JS, Singh V, Lee JK, Lerch J, Ad-Dab'bagh Y, MacDonald D, Lee JM, Kim SI, Evans AC. Automated 3-D extraction and evaluation of the inner and outer cortical surfaces using a Laplacian map and partial volume effect classification. Neuroimage 2005;27(1):210–21, http://dx.doi.org/10.1016/j.neuroimage.2005.03.036.
[24] MacDonald D, Kabani N, Avis D, Evans A. Automated 3-D extraction of inner and outer surfaces of cerebral cortex from MRI. Neuroimage 2000;12(3):340–56.
[25] Lerch JP, Evans AC. Cortical thickness analysis examined through power analysis and a population simulation. Neuroimage 2005;24(1):163–73, http://dx.doi.org/10.1016/j.neuroimage.2004.07.045.
[26] Robbins S, Evans AC, Collins DL, Whitesides S. Tuning and comparing spatial normalization methods. Med Image Anal 2004;8(3):311–23, http://dx.doi.org/10.1016/j.media.2004.06.009.
[27] He Y, Chen Z, Evans A. Structural insights into aberrant topological patterns of large-scale cortical networks in Alzheimer's disease. J Neurosci 2008;28:4756–66.
[28] Benjamimi Y, Hochberg Y. Controlling the false discovery rate: a practical and powerful approach to multiple testing. Journal of the Royal Statistical Society. Series B (Methodological) 1995;57:289–300.
[29] Collins DL, Holmes CJ, Peters TM, Evans AC. Automatic 3D model-based neuroanatomical segmentation. Hum Brain Mapp 1995;3:190–208.
[30] Hinkley DV. Improving the jackknife with special reference to correlation estimation. Biometrika 1978;65:13–22.
[31] Efron B. Nonparametric estimates of standard error: the jackknife, the bootstrap and other methods. Biometrika 1981;68:589–99.
[32] Miller RG. The jackknife — a review. Biometrika 1974;61:1–16.
[33] van Wijk BCM, Stam CJ, Daffertshofer A. Comparing brain networks of different size and connectivity density using graph theory. PLoS One 2010;5(10):e13701, http://dx.doi.org/10.1371/journal.pone.0013701.
[34] Genovese CR, Lazar NA, Nichols T. Thresholding of statistical maps in functional neuroimaging using the false discovery rate. Neuroimage 2002;15(4):870–8, http://dx.doi.org/10.1006/nimg.2001.1037.
[35] Pavlicova M, Santner T, Cressie N. Detecting signals in FMRI data using powerful FDR procedures. Stat Interface 2008;1:23–32.
[36] Amaral L, Scala A, Barthelemy M, Stanley HE. Classes of small-world networks. Proc Natl Acad Sci U S A 2000;97:11149–52.
[37] Watts DJ, Strogatz SH. Collective dynamics of 'small-world' networks. Nature 1998;393(6684):440–2, http://dx.doi.org/10.1038/30918.
[38] Latora V, Marchiori M. Efficient behavior of small-world networks. Phys Rev Lett 2001;87(19):198701.
[39] Latora V, Marchiori M. Economic small-world behavior in weighted networks. Eur Phys J B 2003:249–63.
[40] Bassett DS, Bullmore E. Small-world brain networks. Neuroscientist 2006;12(6):512–23, http://dx.doi.org/10.1177/1073858406293182.
[41] Maslov S, Sneppen K. Specificity and stability in topology of protein networks. Science 2002;296(5569):910–3, http://dx.doi.org/10.1126/science.1065103.
[42] Freeman L. A set of measures of centrality based on betweenness. Sociometry 1977;40:35–41.
[43] Freeman L. Centrality in social networks: conceptual clarification. Soc Netw 1978;1:215–39.
[44] Barthelemy M. Betweenness centrality in large complex networks. Eur Phys J B 2004;38:163–8.
[45] Hampel FR, Ronchetti EM, Rousseeuw PJ, Stahel WA. Robust statistics. An approach based on influence functions. New York: John Wiley and Sons; 1985.
[46] D. Gleich, Matlabbgl: A matlab graph library version 4.0 (2008).
[47] Humphries MD, Gurney K. Network 'small-world-ness': a quantitative method for determining canonical network equivalence. PLoS One 2008;3(4):e0002051, http://dx.doi.org/10.1371/journal.pone.0002051.
[48] Luppino G, Rizzolatti G. The organization of the frontal motor cortex. News Physiol Sci 2000;15:219–24.
[49] Mesulam M. From sensation to cognition. Brain 1998;121:1013–52.
[50] Barabasi A, Albert R. Emergence of scaling in random networks. Science 1999;286:509–12.
[51] He Y, Wang J, Wang L, Chen ZJ, Yan C, Yang H, Tang H, Zhu C, Gong Q, Zang Y, Evans AC. Uncovering intrinsic modular

organization of spontaneous brain activity in humans. PLoS One 2009;4(4):e5226, http://dx.doi.org/10.1371/journal.pone.0005226.
[52] Seeley WW, Crawford RK, Zhou J, Miller BL, Greicius MD. Neurodegenerative diseases target large-scale human brain networks. Neuron 2009;62:42–52.
[53] Hayasaka S, Laurienti PJ. Comparison of characteristics between region-and voxel-based network analyses in resting-state fMRI data. Neuroimage 2010;50:499–508.
[54] Fornito A, Zalesky A, Bullmore ET. Network scaling effects in graph analytic studies of human resting-state FMRI data. Front Syst Neurosci 2010;4:22.